Experiments in Fluids 1, 3–14 (1983)

Experiments in Fluids

© Springer-Verlag 1983

The Influence of Free-Stream Disturbances on Low Reynolds Number Airfoil Experiments

T. J. Mueller, L. J. Pohlen

Department of Aerospace and Mechanical Engineering, University of Notre Dame, Notre Dame, IN 46556, USA

P. E. Conigliaro

Grumman Flight Test Center, F04-007, Calverton, NY 11933, USA

B. J. Jansen, Jr.

McDonnell Douglas Technical Services Company Inc., 16441 Space Center Blvd., Houston, TX 77058, USA

Abstract. The results of an investigation of the influence of free stream disturbances on the lift and drag performance of the Lissaman 7769 airfoil are presented. The wind tunnel disturbance environment is described using hot-wire anemometer and sound pressure level measurements. The disturbance level is increased by the addition of a 'turbulence screen' upstream of the test section and/or the addition of a flow restrictor downstream of the test section. For the Lissaman airfoil it was found that the problems associated with obtaining accurate wind tunnel data at low chord Reynolds numbers (i.e., below 200,000) are compounded by the extreme sensitivity of the boundary layers to the free stream disturbance environment. The effect of free stream disturbances varies with magnitude, frequency content, and source of the disturbance.

List of Symbols

c_d	section profile drag coefficient
c_l	section lift coefficient
R_c	Reynolds number based on airfoil chord and free stream conditions
u_{RMS}	root-mean-square of the fluctuating velocity, m/s
U	test section velocity, m/s
x	distance measured from beginning of test section, cm
$\bar{x}$	distance measured along airfoil chord from the leading edge divided by chord length, percent
α	angle of attack, degrees

Subscripts

max	maximum value
min	minimum value

1 Introduction

Recently, attention has turned toward low Reynolds number airfoil design in an effort to obtain better performance for a variety of practical applications. Low chord Reynolds numbers occur when there is a low free stream velocity, a low air density, or a small airfoil chord. Applications where one or more of these conditions are present include jet engine fan blades, remotely piloted vehicles (RPV's) at high altitudes, sailplanes, ultra-light man-carrying/man-powered aircraft, and mini-RPV's at low altitudes. These systems require efficient airfoil sections in the chord Reynolds number range from about 100,000 to about 1,000,000.

Many significant aerodynamic problems occur below chord Reynolds numbers of about 500,000 as discussed by Mueller and Batill (1980). These problems are related to the management of the airfoil boundary layer and the difficulties associated with making accurate wind tunnel (Mueller and Jansen 1982) and free flight measurements (Miley 1972). In relation to the airfoil boundary layer, important areas of concern are the separated regions which occur near the leading and/or trailing edges and transition from laminar to turbulent flow (Mueller and Batill 1980). It is well known that separation and transition are highly sensitive to Reynolds number, pressure gradient, and the disturbance environment (Schlichting 1979). Transition and separation play a critical role in determining the development of the boundary layer which, in turn, affects the overall performance of the airfoil.

The disturbance environment present in the test section of a low speed wind tunnel is usually determined by free stream turbulence (velocity fluctuations), acoustic phenomena (pressure fluctuations) and mechanical vibrations. The free stream turbulence level depends on the history of the flow in the settling chamber, flow straightners or screens and inlet leading to the test section. Acoustic phenomena are related to the noise emitted from turbulent boundary layers on the side walls, unsteady separated flow regions and, the fan and its associated drive system. Mechanical vibrations may be caused by rigid coupling of the fan and drive system to the wind tunnel as well as the unsteady wakes of probe and model supports. Although these factors which determine the disturbance environment may be reduced and controlled, they cannot be completely eliminated. It is apparent that, in general, each wind tunnel has a different disturbance environment

which is a function of its design and method of fabrication. Because the airfoil boundary layers are sensitive to small disturbances, accurate wind tunnel models are very important in the evaluation of a given design. Furthermore, because the forces, pressure differences and velocities are small, a great deal of care must be exercised to obtain accurate and meaningful data. It is not surprising therefore, that similar experiments on the same geometry model at low Reynolds numbers often produce results which differ from one wind tunnel to the next. This research was performed in a continuing effort to understand the influence of wind-tunnel free-stream disturbances on low Reynolds number airfoil experiments.

2 Experimental Apparatus and Procedure

This research was conducted in the Aerospace Laboratory of the University of Notre Dame. The equipment used consisted of a wind tunnel and a strain gauge balance with its associated electronics for lift and drag measurements, electronic manometers and, a micro-computer system. A hot-wire anemometer and sound pressure level analyzer were used to describe the test section environment. The flow visualization studies used the smoke tube method, strobe lights, and camera described by Mueller (1979).

2.1 Airfoil Models

The airfoil section used for this study was the Lissaman 7769 profile described by Burke (1980). This 11% thick airfoil section was designed for a chord Reynolds number of approximately 600,000 and used for the Gossamer Condor and Albatross man-powered aircraft. The geometry and coordinates of this airfoil section are shown in Fig. 1 and Table 1 respectively. The model was constructed of wood using two steel end plates machined to the profile of the airfoil. Spanwise steel reinforcing rods were added for strength. The wood was coated with an epoxy and finished to give a smooth surface. Finally the model was given several coats of flat black paint to provide good contrast for the smoke visualization studies. The airfoil model had a 437 mm span and a 249 mm chord.

Table 1. Coordinates of the Lissaman 7769 airfoil from Burke (1980)

All Values in Percent Chord

$\bar{x}$	upper surface	lower surface
0	0	0
1.25	2.25	−1.64
2.5	3.34	−2.01
5.0	4.96	−2.30
7.5	6.15	−2.30
10	7.06	−2.16
15	8.40	−1.70
20	9.26	−1.38
30	9.92	−1.06
40	8.97	−0.91
50	6.96	−0.75
60	4.86	−0.60
70	3.16	−0.45
80	1.81	−0.30
90	0.84	−0.16
95	0.41	−0.08
100	0	0

Nose radius 1.84, center of nose circle (1.84, 0.14); Trailing edge angle from chord line upper surface 4.5°, lower surface −0.9°

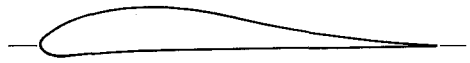

Fig. 1. Lissaman 7769 Airfoil Geometry

2.1 Wind Tunnel and Balance

The wind tunnel used was a non-return, low speed tunnel designed by F. N. M. Brown. It is capable of maintaining low turbulence intensities ($u_{RMS} \times 100/U \approx 0.10\%$) over the normal range of tunnel velocities, 9 m/s to 30 m/s. A schematic of the Notre Dame wind tunnel is shown in Fig. 2. Twelve anti-turbulence screens break up swirling air as it enters the contraction cone. The contraction cone is square in cross-section and has a contraction ratio of 24 : 1. Test sections are interchangeable; the size used was 610 mm square (24″ × 24″) an 1828 mm long (72″). The test section and diffuser are separated by a 101 mm wide foam rubber insulator to damp vibrations from the motor. An eight-bladed fan is driven by a 15 H. P. AC motor with variable speed drive. The motor and fan unit are mounted outside the Aerospace Lab and are isolated from the diffuser structure. A small enclosure protects this equipment from the elements.

The lower limit of the tunnel velocity was normally 9 m/s, but this could be extended to as low as 2.1 m/s by the addition of one or two flow restrictors between the vibration insulation and the test section (shown in Fig. 3). The flow restrictors were made from ordinary plastic drinking straws, 55 mm I. D. by 200 mm long packed with

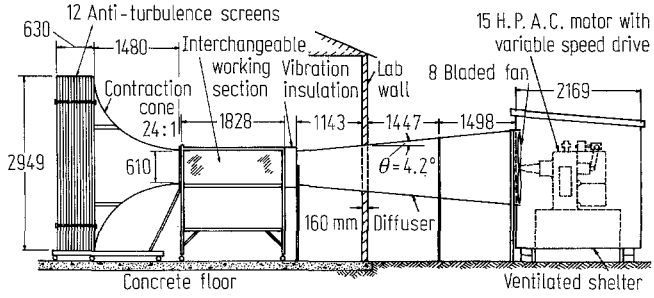

Fig. 2. Low turbulence subsonic wind tunnel

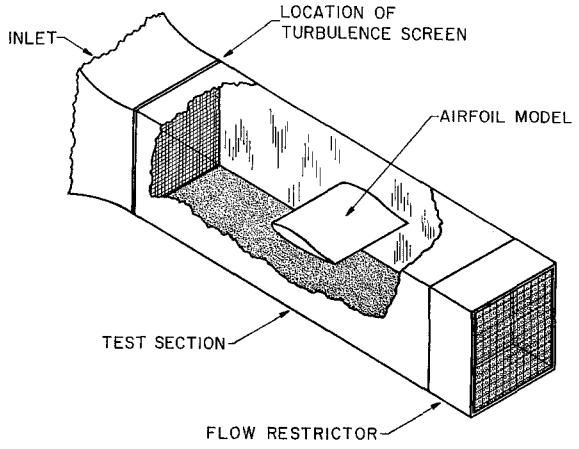

Fig. 3. Test section showing the turbulence screen and flow restrictor locations (airfoil side plates not shown)

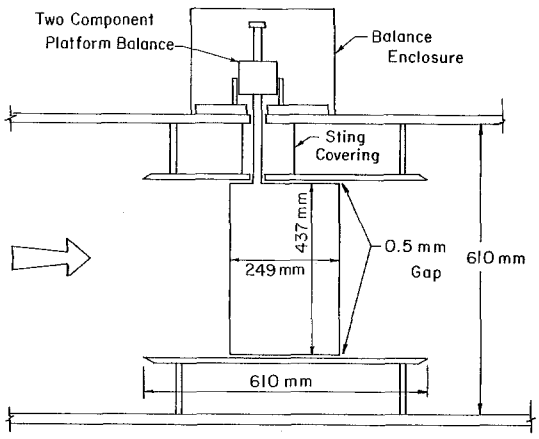

Fig. 4. Test section showing airfoil, force balance and side plate arrangement

the length running in the streamwise direction. The pressure drop through the straws reduced the test section velocity and also helped damp out undesired fluctuations caused by outdoor wind variations. In order to produce higher turbulence intensities in the test section, a wire mesh 'turbulence screen' was placed between the tunnel inlet and the test section (Fig. 3). For this study a single screen with 7.09 meshes/cm and a wire diameter of 0.245 mm producing a free-stream turbulence intensity of about 0.30% was used. The standard wind tunnel with no screen produced a turbulence intensity of 0.08%. The screen location is illustrated in Fig. 3.

The test section used to take lift and drag force data had an externally mounted, two-component strain gauge balance. The balance operated on a two flexure system, with a sensitive flexure being engaged for low loads (as small as 0.01 N or 0.04 ounces). A second, stiffer flexure was engaged at approximately 12.74 N (46 ounces). A pulley arrangement was used to calibrate the balance. Weigths were placed in a basket which was connected over the pulley to the balance sting. This provided the relationship between the applied force and the voltage output of the strain gauge balance amplifier. The angle of attack of the model was changed with a motor and gear arrangement which could be set to less than ± 0.05 degrees. The force test model was mounted vertically between two plates, one glass and one aluminum which measured 13 mm × 610 mm × 610 mm (1/2″ × 24″ × 24″). One of these plates was fixed on the top wall of the test section and a fairing was placed around the sting to isolate it from tunnel flow. The second plate was mounted on supports above the test section floor so that the airfoil model 'floated' between the plates. The gaps between the model and end plates were held as close as possible to 0.51 mm (0.020″) to minimize leakage of flow through the gaps but preventing contact with the plates during the tests. This two-dimensional configuration approximated an airfoil with an effective aspect ratio of infinity. Figure 4 shows this arrangement.

The velocity in the test section was determined either by using a pitot-static tube mounted upstream and above the model or by measuring the static pressure at the entrance to the test section. For dynamic pressures under 14 mm (0.5536 inches) of water, a Setra Systems (Model 339 B) electronic manometer was used because of its accuracy in this low range. To measure dynamic pressures greater than 14 mm of water, a Setra Systems Model 339 H (with range to 127 mm or 5.0 inches of water) was used. Both manometers had a differential transducer with an accuracy of $\pm 0.2\%$ of the reading. The amplified, filtered outputs of the strain gauges along with the free stream velocity from the electronic manometer were then processed by an Apple II Plus data acquisition system.

2.3 Instrumentation for Turbulence Measurements

A hot-wire anemometer system was used to determine mean tunnel velocities and turbulence intensities in the test section under varying test conditions. All hot wire measurements were made by a DISA Type 55P11 hot-wire probe, with a sensing element 5 microns in diameter and 1.5 mm long. The hot-wire anemometer system consisted of the DISA 55M10 constant-temperature anemometer which could be tuned to respond to frequencies up to 50,000 Hz with a hot-wire operating temperature between 250 °C and 300 °C. A DISA 55D10 linearizer was used and adjusted so that voltage output of the anemometer corresponded directly to the tunnel speed. Previous studies conducted at the Notre Dame Aerospace Laboratory by Kegelman (1982) showed that the linearizer produced a small amount of electronic noise which became a significant part of the total turbulent signal at turbulent intensities below 0.1%. The output of the linearizer was monitored on a Data Precision Corporation V-45 Digital voltmeter to obtain tunnel velocities. Simultaneously, the output signal was filtered and amplified. The DC component was filtered out using a 1 Hz high pass filter and the

remaining AC component was amplified to produce a useful voltage on a T.S.I. Model 1076 true RMS meter, which (knowing the amplification) yielded the root-mean-square turbulence intensity, $u_{RMS} \times 100/U$. When taking data for frequency analysis, the DISA linearizer was by-passed in order to eliminate any 60 cycle noise from the frequency spectrum. All analog voltage outputs were sampled using the A/D capabilities of the Apple II microcomputer and associated software developed specifically for these experiments.

2.4 Instrumentation for Acoustic Measurements

Sound pressure level measurements were accomplished through the use of a Bruel and Kjaer Frequency Analyzer type 2107. The type 2107 is an AC operated audio frequency analyzer of the constant percentage band-with type. Although designed as a narrow band sound and vibration analyzer, it may be used for any kind of frequency analysis within the range of 20–20,000 Hz. The frequency analyzer was combined with a Bruel and Kjaer Level Recorder Type 2305, allowing frequency amplitude diagrams to be recorded automatically on preprinted frequency calibrated paper. The Selective Amplifier Section of the sound pressure level equipment was used as a narrow-band analyzer which could be continuously varied from 20 to 20,000 Hz. The octave selectivity was set at 45 decibels to produce the narrowest possible bandwith of approximately 1/3 octave. Two different condenser microphones were used in the analysis. All of the testing was accomplished with the use of a Bruel & Kjaer Nose Cone UAO386 designed to reduce the aerodynamically induced noise present when the microphones are exposed to high wind speeds. The nose cones were designed to replace the normal protection grid of the microphone cartridge and were of a highly streamlined shape with a highly polished surface. A fine wire mesh around the circumference of the cone allowed sound waves to penetrate to the microphone diaphragm. As most of the tunnel noise was propagated upstream from the fan blade the directional characteristics of the microphone were an important consideration. Bruel and Kjaer (1960) describe the omnidirectional characteristics of the microphone when the nose cone is used. Any body regardless of how streamlined produces some aerodynamically induced noise. For the purposes of this study it was assumed that the aerodynamic noise produced by the microphone with its nose cone would not exceed the aerodynamic noise produced by any similarly streamlined body and the results should thus give a reasonable indication of the acoustic environment.

2.5 Data Acquisition System

The data acquisition system used with the strain gauge force balance, hot-wire anemometer and sound pressure level systems consisted of an Apple II Plus microcomputer and the associated hardware necessary to give the computer analog-to-digital (A/D) capabilities. An Interactive Structure Inc. Model AI13 analog input system was the primary signal processing device used to give the Apple II microcomputer its data acquisition capabilities. The 12 bit capability of the converter produced a resolution of 0.05 mv at small voltages. For measuring and recording fluctuating signals the AI13 converter was capable of sampling rates as high as 22,000 samples per second for short strings of data.

2.6 Experimental Procedure

All measurements were made in the South Tunnel at the University of Notre Dame Aerospace Laboratory. The force balance was used to collect lift and drag data on the Lissaman airfoil over a angle of attack range of –20° to 25°. The tunnel was always started with the airfoil at 0° angle of attack. All data were corrected for solid body blocking, wake blocking, streamline curvature and longitudinal buoyancy according to the methods described by Rogers (1966). Once the tunnel was on, the angle of attack was changed to –20° and the experiment was conducted increasing the angle of attack with the tunnel running. The test was concluded by decreasing the angle of attack from 25° back to 0° again while the tunnel was running. At each angle of attack the microcomputer sampled the lift and drag and electronic manometer simultaneously over a 5 second period taking 100 samples to be averaged. Zero lift and drag voltages were measured just prior and immediately after the experiment to account for any amplifier drift. The data was corrected for this drift based on a linear drift during the period of the experiment. Calibration of the force balance was checked every fourth test. The force/voltage calibration remained constant over long periods of time.

Both the hot-wire and sound level measurements (68 cm downstream from the entrance to the test section) were taken at a location 8 cm ahead of the leading edge of the airfoil. For convenience the model was removed when free-stream measurements were made. Figure 3 shows the experimental set-up with location of flow-restrictor and turbulence screen.

Previous studies by Jansen (1982) and Kegelman (1982) have shown that free-stream turbulence and sound levels at a given streamwise location are invarient across the test section except at locations near the wall. In this study the probes were centered in the test section between the side-plates at a height comparable with the location of the leading edge of the airfoil model.

Measurements were made over a velocity range of 2.5 to 31 m/s with different combinations of the turbulence screen and flow restrictors. The hot-wire anemometer was used to monitor free-stream velocity, measure free-stream

turbulence intensities, and determine frequency content of the turbulent velocity fluctuations. Frequency spectra were obtained by sampling the hot-wire anemometer signal acquiring 1024 samples at a specified sampling rate. The sampling rate could be specified to increase the frequency resolution at low frequencies or to increase the overall frequency range capability. Two frequency spectra were taken at each testing point, one over a range of 0 to 500 Hz with a resolution of 0.98 Hz and the other over a range of 0 to 5000 Hz with a resolution of 9.8 Hz.

The Bruel and Kjaer frequency analyzer was used to determine total sound pressure levels in the test section. Calibration of the frequency analyzer was accomplished with a 124 decibel B & K pistonphone prior to testing. The pistonphone produced a constant 124 decibel sound level with a primary frequency of 250 Hz. Microphone calibration was checked periodically and no drift was observed. The frequency content of the sound field was documented by making filtered measurements of the sound level from 20 to 2,000 Hz using the selective amplifier as a narrow-band analyzer. Frequency content of the sound field was also obtained by sampling the microphone output directly and performing the same analysis as described for the hot-wire signal. A comparison of the two methods shows an excellent correlation.

Finally, to analyze the data it was necessary to know the frequency of the fan blade passage. This was obtained for each velocity and test condition by marking a single fan blade with a piece of tape and using a hand-held strobe to determine the fan blade rpm.

3 Disturbance Environment – no Airfoil Present

Results of the acoustic and turbulence measurements showed that the experimental environment was a complex function of many variables. Measurements were made to take into account as many of these variables as was possible. Figures 5 and 6 present the freestream turbulence

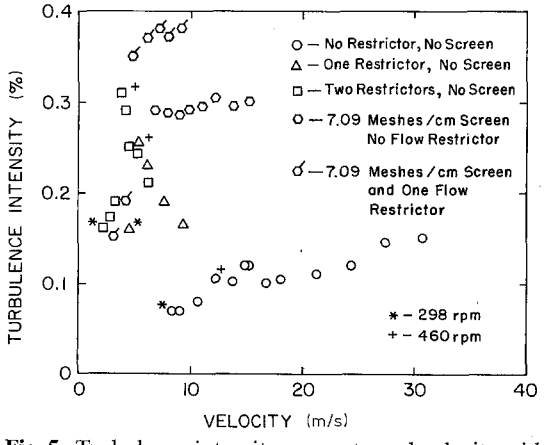

Fig. 5. Turbulence intensity versus tunnel velocity with and without flow restrictors and screen

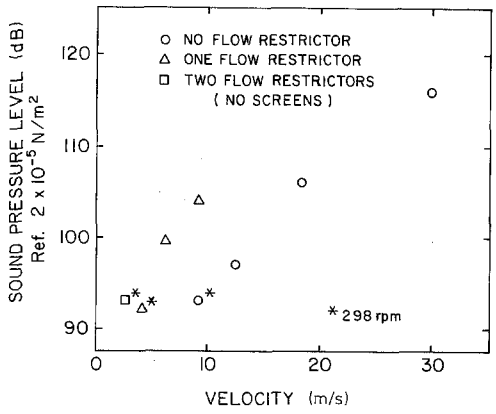

Fig. 6. Sound pressure level versus tunnel velocity with and without flow restrictors

intensities and sound pressure levels over the entire range of velocities. In the velocity range from 9 to 31 m/s no flow restrictors were used. The turbulence intensity varys from 0.07% to 0.15% in this range. Turbulence intensities as low as 0.05% were calculated using analytical techniques to reduce the hot-wire data. In using the linearizer to measure turbulence intensities electronic noise was introduced which increased the measurements slightly. Therefore actual turbulence intensities may be slightly lower than those presented here. A comparison of turbulence intensities calculated analytically with those from the linearizer above intensities of 0.15% show good agreement since the electronic noise was no longer a significant addition to the turbulent signal.

There was a noticeable increase in turbulence intensity at a velocity of 12 m/s. This corresponded to a fan rpm of approximately 460. At this fan rpm there was a marked pulsating of the fan blades as the belt-drive from the motor appeared to slip at this setting. The pulsating of the fan was accompanied by a slight squeaking of the belts. When a flow restrictor was introduced the turbulence intensities in the section were increased significantly. The turbulence intensity at idle speed (i.e., 298 rpm) increased from 0.07% to 0.16% when one or two flow restrictor were used (Fig. 5). With one flow restrictor a large increase in turbulence was observed at 5.5 m/s while an even larger increase was observed at 3.8 m/s when two flow restrictors were in place. Both of these velocities corresponded to a fan rpm of about 460. It may be the increased work load in conjunction with the pulsating tendency of the fan at this rpm which causes the fan to induce these high turbulence intensities in the test section. The u_{RMS} remains essentially the same and the decrease in U causes the ratio of u_{RMS}/U to increase. Once the 460 rpm region is passed the turbulence intensities gradually decreased but always remain higher than the no flow restrictor case. An important comparison can be made at 9 m/s (approximately 150,000 chord Reynolds number for the Lissaman Airfoil) where the tunnel may be operated with no flow restrictor

or with one flow restrictor in place. The turbulence intensity increases from 0.07% to 0.16% when one flow restrictor was inserted after the test section as shown in Fig. 5.

Analysis of the sound pressure levels in the test section indicated a different behavior. Sound levels at idle remained constant at approximately 93 dB (referred to 2×10^{-5} N/m^2) regardless of the experimental set-up (Fig. 6). Introduction of flow restrictors or a turbulence screen did not appear to change the total sound pressure level in the test section for a given fan rpm. However, to achieve the same test section velocity with one flow restrictor in place the fan had to be operated at a higher rpm. When operating at a chord Reynolds number of 150,000 with one flow restrictor in place, a total sound level of 104 dB was measured in the section compared to a much quiter 93 dB at the same velocity with no flow restrictor in use. Special care was taken to visually observe the probes for mechanical vibrations which may have been produced by tunnel vibrations or the flow over the probe holders. The foam insulation between the test section and tunnel diffuser successfully damped any mechanical vibrations from the fan motor and no vibration of either the hot-wire or microphone probes was observed.

Introduction of a turbulence screen between the test section and tunnel inlet increases the turbulence intensity in the test section. Figure 5 shows a comparison of turbulence intensities produced by a single turbulence screen with 7.09 meshes/cm both with and without one flow restrictor in place. The lowest set of points represent the case with no turbulence screens (i.e., the standard wind tunnel configuration). At very low speeds with both screen and one flow restrictor in place, the screen did not induce turbulence intensities much higher than those present due to the flow restrictor alone. As the speed increased the turbulence intensity increased significantly. Turbulence intensities produced by the turbulence screen with the flow restrictor in place were larger than turbulence intensities produced with the turbulence screen alone over the same velocity range. This suggests that the total turbulence intensity may be due to a coupling of the velocity and acoustic fields.

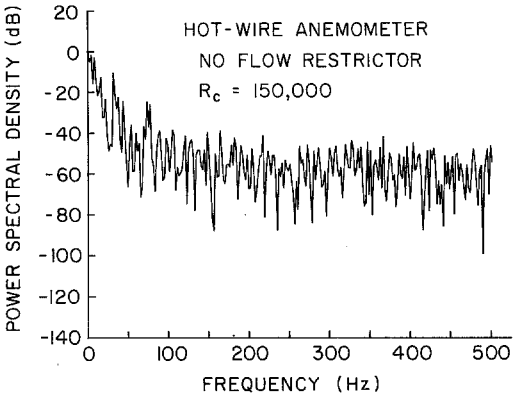

Fig. 8. Power spectral density versus frequency at $x=68$ cm, $U=9$ m/s and no flow restrictor from hot-wire anemometer

Total turbulence intensity and sound pressure levels reveal many important facts about the test section environment. In order to determine the source of the acoustic and turbulent phenomona in the test section, an analysis of their frequency spectra is required. In addition, it is well known that the presence of characteristic frequencies in the freestream can effect the transition of a laminar boundary layer and thereby radically change the results of the experiment.

The frequency spectra presented here correspond to a chord Reynolds number of 150,000 on the Lissaman Airfoil (approximately 9 m/s). Frequency analysis was conducted with both the sound pressure level equipment and the hot-wire anemometer. Figures 7 and 8 present frequency spectra at $R_c=150{,}000$ for the standard wind tunnel configuration from the sound and hot-wire analysis respectively. In these figures, as well as Fig. 9 through 12, the frequency spectra presented were normalized with the maximum value for the case considered. Both the sound and hot-wire equipment picked up the fan blade passage frequency of 42 Hz. This frequency was a major part of

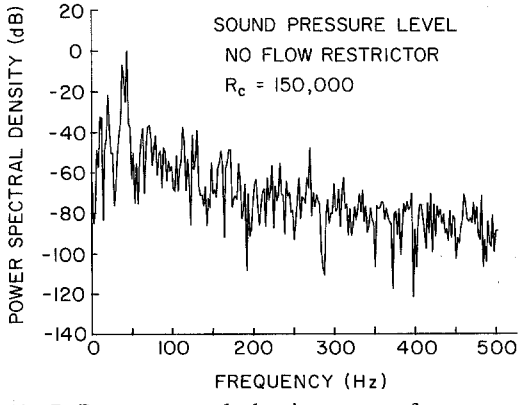

Fig. 7. Power spectral density versus frequency at $x=68$ cm, $U=9$ m/s, and no flow restrictor from sound measurements

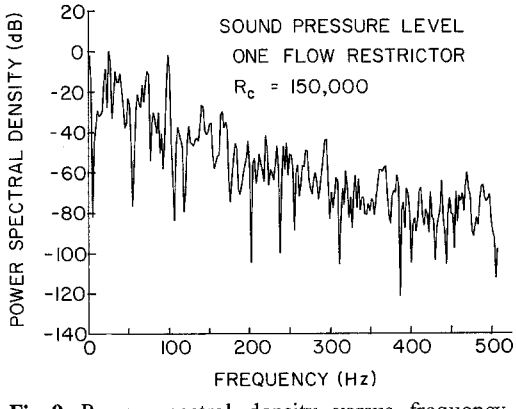

Fig. 9. Power spectral density versus frequency at $x=68$ cm, $U=9$ m/s and one flow restrictor from sound measurements

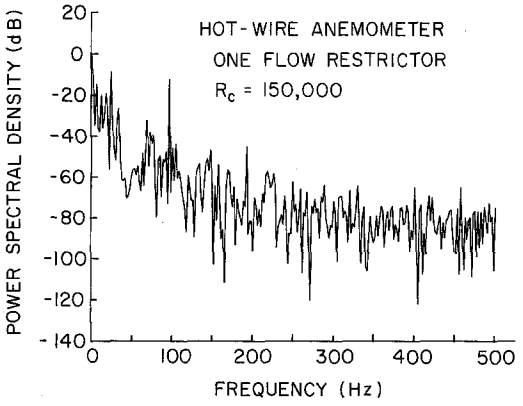

Fig. 10. Power spectral density versus frequency at $x=68$ cm, $U=9$ m/s and one flow restrictor from hot-wire anemometer

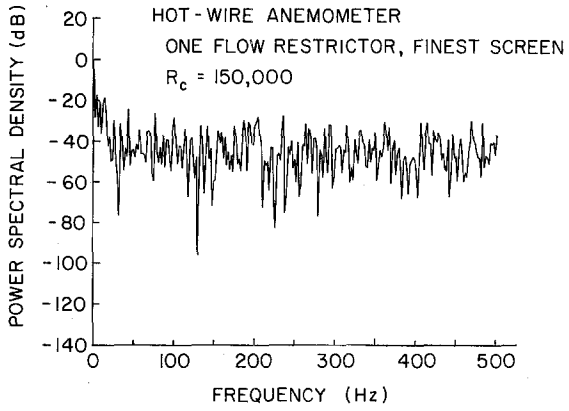

Fig. 11. Power spectral density versus frequency at $x=68$ cm, $U=9$ m/s, one flow restrictor and one 7.09 meshes/cm screen from hot-wire anemometer

the acoustic signal. While still significant in the turbulent signal, it can be seen that lower frequencies add a substantial amount of turbulence in addition to the fan blade passage. These lower frequencies may include a slight pulsating of the fan which would fall in this lower range of frequencies. Some harmonics of the primary frequency can be seen in both the hot-wire and acoustic signals. Figures 9 and 10 are frequency spectra taken at the same tunnel velocity with one flow restrictor in place. The fan blade passage frequency has increased to about 100 Hz as the fan operates at a higher speed to compensate for the pressure loss through the flow restrictor. A lower frequency of 25 Hz has also appeared. This frequency is twice the fan rpm and becomes prevalent due to the slight pulsating of the fan under the increased work load. Under these test conditions the acoustic phenomena have become a larger part of the turbulent signal. The frequencies associated with the fan blade passage become the primary frequencies of the turbulent signal as seen in Fig. 10. The lower frequencies are still present but are of the same or lower magnitude as the fan blade frequencies.

Thus, part of the increase in turbulence intensity resulting from the introduction of a flow restrictor is apparently due to an increase in sound pressure level. Characteristic frequencies in the freestream at a given velocity (i.e. Reynolds number) will also vary depending on whether a flow restrictor is used.

Finally, with the introduction of a turbulence screen with 7.09 meshes/cm in the flow, the frequency spectrum becomes broadband with no characteristic frequencies for both the flow restrictor and no flow restrictor cases (Fig. 11, 12). The turbulence levels introduced by the screens are much higher than the free-stream disturbances caused by the fan blade passage or any pulsating of the fan. For the $R_c=150{,}000$ case the introduction of a turbulence screen dominated the test section environment. This does not mean the acoustic effects are absent only that the order of this disturbance is much lower than that produced by the turbulence screen. Figures 13, 14, and 15 show sound level frequency spectra obtained from the B & K 2107 frequency analyzer. Calibration curves provided with the nose cone microphone show that aerodynamic noise was concentrated in the 30 to 50 Hz range and this was confirmed by the data obtained. Figure 13 shows the frequency spectrum produced at $R_c\approx150{,}000$ using no flow restrictor and no turbulence screen. Aerodynamic noise is prevalent but the characteristic fan blade passage frequency of 40 Hz is still visible. A higher harmonic around 78 Hz is also present. Figure 14 shows the frequency spectrum with the introduction of one flow restrictor. The acoustic frequencies of 25 and 100 Hz clearly dominate the spectrum confirming the previous results and suggesting that the introduction of a flow restrictor amplifies these frequencies in the test section. Figure 15 shows the frequency spectrum with the turbulence screen in place. Aerodynamic noise was increased and may be the result of a turbulent boundary layer on the microphone head. Acoustic fan blade frequencies were present but not amplified over the empty tunnel conditions.

A better understanding of the conditions present in the test section when flow restrictors were introduced to

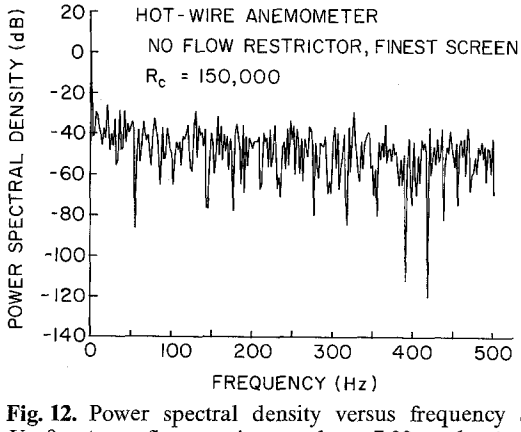

Fig. 12. Power spectral density versus frequency at $x=68$ cm, $U=9$ m/s, no flow restrictor and one 7.09 meshes/cm screen from hot-wire anemometer

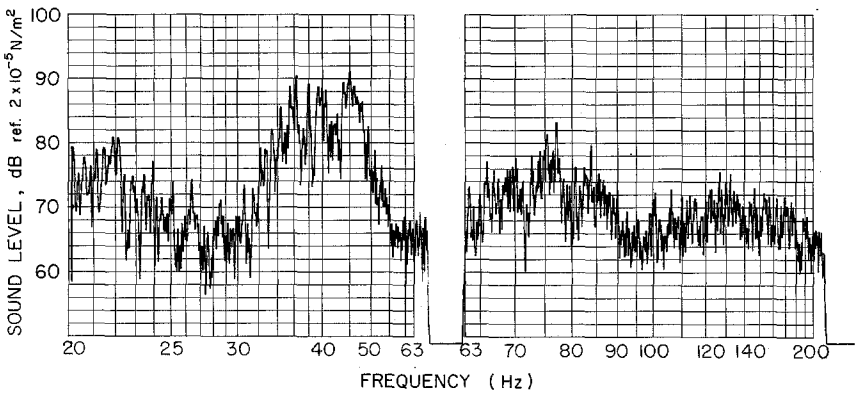

Fig. 13. Sound pressure level from 2107 frequency analyzer at $R_c = 150{,}000$ (no flow restrictor, no screen)

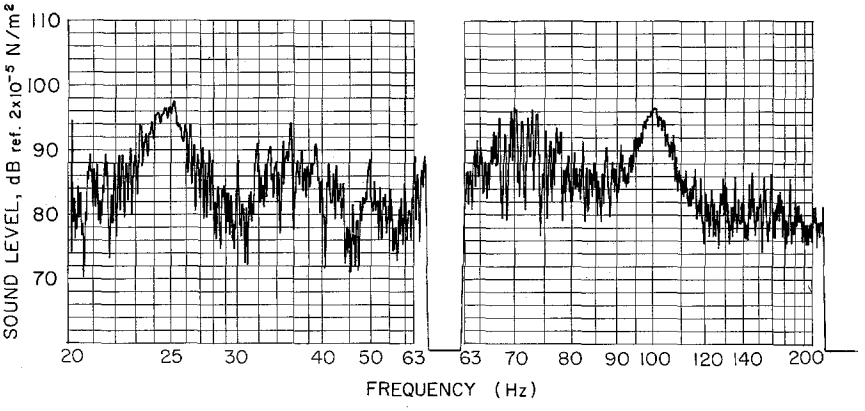

Fig. 14. Sound pressure level from 2107 frequency analyzer at $R_c = 150{,}000$ (one flow restrictor, no screen)

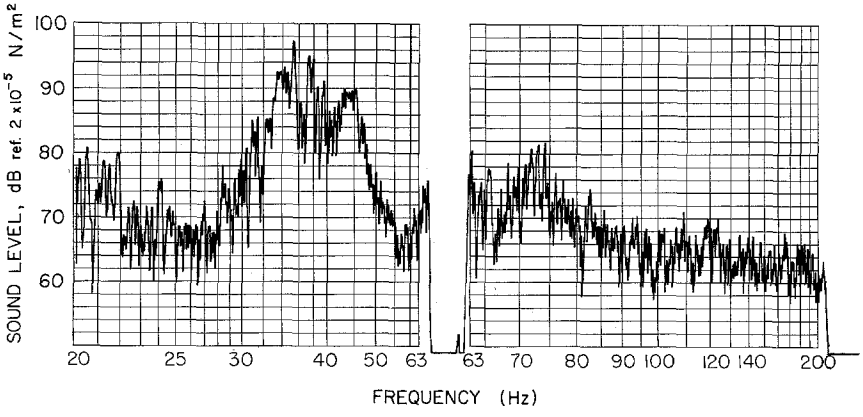

Fig. 15. Sound pressure level from 2107 frequency analyzer at $R_c = 150{,}000$ (no flow restrictor, one 7.09 meshes/cm screen)

reduce the test velocity has been obtained. The purpose of introducing the flow restrictor into the test section was to reduce the Reynolds number of the test. It was found that some of the earlier results attributed to lower Reynolds number may be a result of higher turbulence intensities in the test section. Understanding of the small changes in test environment are critical at these low Reynolds numbers. With the introduction of flow restrictors in the test section turbulence intensities increased significantly. A part of this increase appeared to be caused by the 'amplification' of the sound pressure waves transmitted upstream from the fan blade passage. The increase in turbulence intensity at a fan rpm of 460 was much larger than at any other speed. A combination of increased work load due to the pressure drop through the flow restrictor along with a slight misadjustment of the drive belts caused pulsating of the fan blade and subsequent increased in turbulence. The increase in turbulence produced by the flow restrictors had

very characteristic frequencies. These frequencies varied depending on test conditions. The fan rpm required to achieve a certain test section velocity was dependent on the atmospheric conditions; temperature and barometric pressure. The fan rpm also varied with the outdoor wind velocity which impinged on the fan. Another factor which was found to affect fan rpm was small changes in lab pressure caused by long periods of testing at high speeds. The aerospace laboratory is not air tight. However, high speed testing lowered the lab pressure enough to require increased fan rpm to maintain a constant velocity. This affect was especially noticeable with flow restrictors in place.

In contrast to the increase in turbulence intensity produced by the flow restrictors, turbulence increases due to the introduction of a turbulence screen had no characteristic frequencies in the range studied and the intensities were relatively constant over the complete range of velocities. Turbulence produced by the turbulence screen dominated over that produced by the flow restrictor when it was used in combination with the exception of very low velocities. With the knowledge of these experimental conditions a better understanding of data taken at low Reynolds numbers can be made.

4 Airfoil Performance

The lift and drag performance of the smooth Lissaman airfoil in the standard wind tunnel configuration (Fig. 2) is shown in Fig. 16. As the angle of attack was increased, smoke visualization indicated that at 6° the laminar boundary layer separated on the upper surface at about 25% chord while at 8° the boundary layer appeared to be undergoing transition and separated from the upper surface at about 35% chord. At an angle of attack of 10° transition appeared to be complete and the boundary layer remained attached until about the 70% chord location. There is a noticeable change in the lift curve slope associated with the extension of attached turbulent flow. A smoke photograph at $\alpha = 12°$ is shown in Fig. 17a. The lift coefficient continues to increase in this region, Fig. 16a, until it reaches a maximum value of 1.3 at 16°. Further increases in angle of attack cause the location of turbulent separation near the trailing edge to move upstream and c_l to decrease slightly until it reaches about 35% chord where a jump takes place to a laminar separation at the leading edge at about 19°. At this point there is an abrupt decrease in c_l from about 1.25 to about 0.9. As the angle of attack is decreased from 25°, the boundary layer separates in the laminar state and the c_l remains about 0.9 until an angle of 11° is reached. With little or no free stream turbulence present the very short laminar boundary layer separates from the airfoil before transition takes place. A comparison of the airfoil flow field at $\alpha = 12°$ for both increasing and decreasing angle of attack is shown in Fig. 17. The lift jumps up at $a = 10°$ as a result of the fact that transition in the separated shear layer allows the flow to reattach. The accompanying variation in the profile drag coefficient is shown in Fig. 16b. The abrupt decrease in c_l is accompanied by an abrupt increase in c_d. Therefore in the lowest turbulence, quietest wind tunnel configuration, a significant hysteresis region in the lift and drag forces was found. The presence and extent of this hysteresis was determined by the location of separation and/or transition in the boundary layer. The location of transition from laminar to turbulent flow in the boundary has been known to be affected by the level and type of free stream disturbances for a long time (Schlichling 1979).

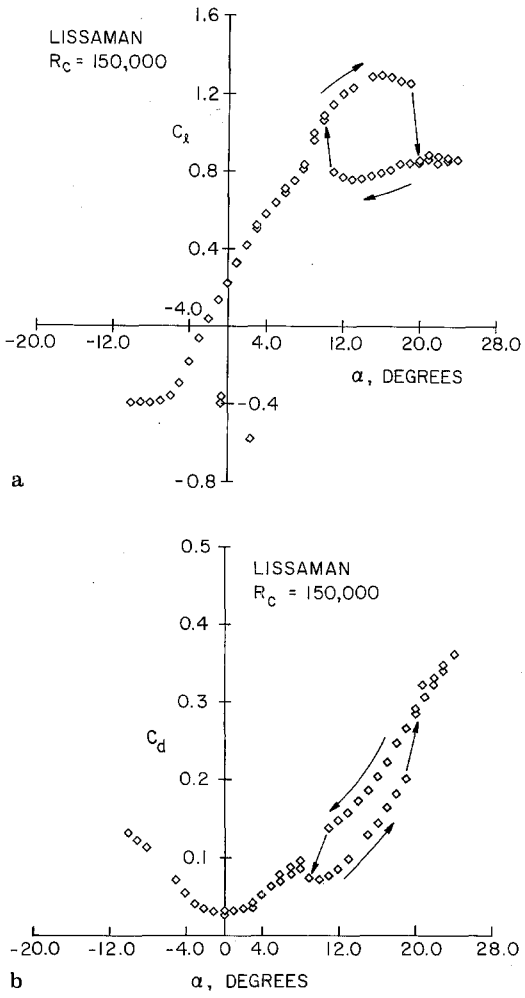

Fig. 16a and b. Lift and drag coefficients versus angle of attack of the smooth Lissaman airfoil with no screen or flow restrictor (hysteresis); **a** section lift coefficient; **b** section profile drag coefficient

In earlier experiments using this airfoil by Conigliaro (1983), hysteresis was not found. These data were taken by increasing the angle of attack from −10° to +20° angle of attack and then turning the tunnel off for the balance calibration. The airfoil was then returned to −10° angle of attack for the next experiment. In the present investigation no attempt was made to determine whether or not hysteresis occurred at negative angles of attack.

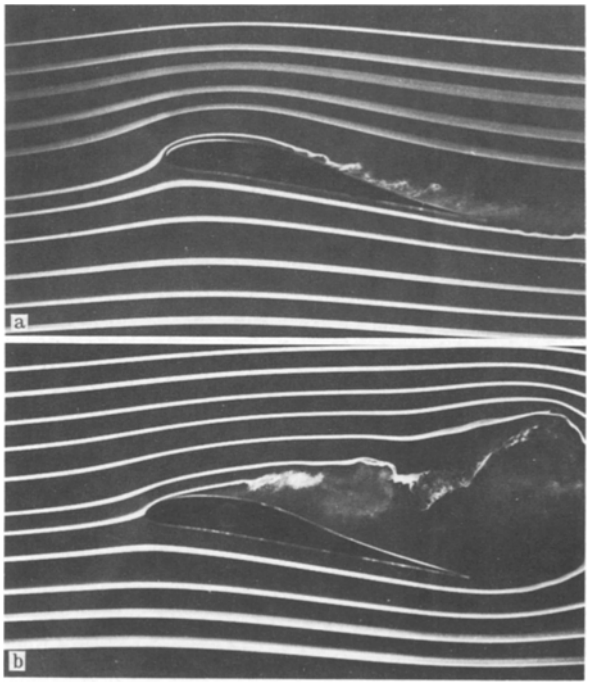

Fig. 17a and b. Smoke photographs of Lissaman airfoil at R_c= 150,000 at 12° angle of attack with no flow restrictor or screen; **a** increasing angle of attack; **b** decreasing angle of attack

The result of changing the accoustical environment by adding one flow restrictor at the end of the test section is shown in Fig. 18. As shown in Figs. 5 and 6, the addition of one restrictor increases both the free stream turbulence level and the sound pressure level for a fixed value of tunnel velocity. This test section environment reduced the size of the hysteresis region and produced a slightly higher $c_{l\max}$ of almost 1.4. A slightly lower minimum drag coefficient was also obtained. The use of two flow restrictors produced similar results with the hysteresis being almost completely eliminated. The increase in free stream turbulence and acoustic excitation caused the laminar shear layer to transition much earlier, thus allowing the flow to reattach sooner.

Increasing the free stream turbulence level to about 0.3%, by adding one 7.09 meshes/cm screen at the upstream end of the test section with no flow restrictor, produced the lift and drag coefficients presented in Fig. 19. This test section environment completely eliminated the hysteresis region and yielded values of $c_{l\max}$ and $c_{d\min}$ between those of Figs. 16 and 18. With a larger turbulence intensity in the test section, the airfoil boundary layer transitions very close to the leading edge, eliminating hysteresis by enabling the flow to reattach at higher angles of attack. The abrupt decrease in c_l occurred at approximately the same angle of attack in each case. The very large adverse pressure gradient at this angle of attack (i.e. 19°) caused the boundary layer to separate whether it was laminar or turbulent. Hysteresis occurred because the laminar separated shear layer did not reattach. An increase in turbulence did not prevent the abrupt loss of lift, but the separated flow was turbulent allowing more rapid reattachment.

When the chord Reynolds number was increased to 200,000 the hysteresis region was reduced when using the standard wind tunnel configuration. At this condition the abrupt decrease in lift occurred at about 19° for increasing angle of attack and the lift jumped up when the angle of attack as decreased to 16°. At a chord Reynolds number of 300,000 the abrupt decrease in lift occurred at about 21° and jumped back up at about 20°.

The importance of this hysteresis phenomena cannot be overemphasized. Low Reynolds number airfoil data obtained in noisy and/or high turbulence wind tunnels may not exhibit significant hysteresis. Therefore, aircraft designed using such wind tunnel data may not perform as expected in flight where the free stream disturbance level is usually very low.

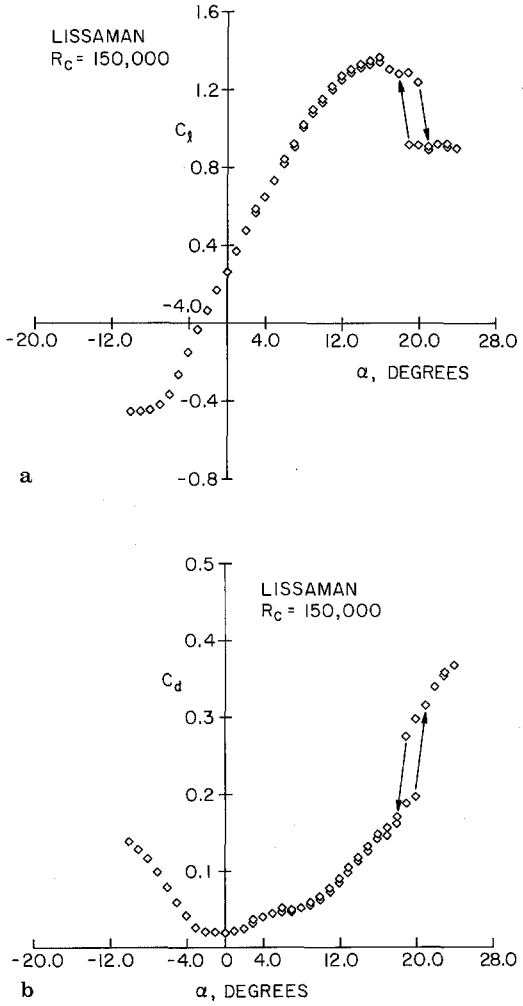

Fig. 18a and b. Lift and drag coefficients versus angle of attack of the smooth Lissaman airfoil with no screen and one flow restrictor; **a** section lift coefficient; **b** section profile drag coefficient

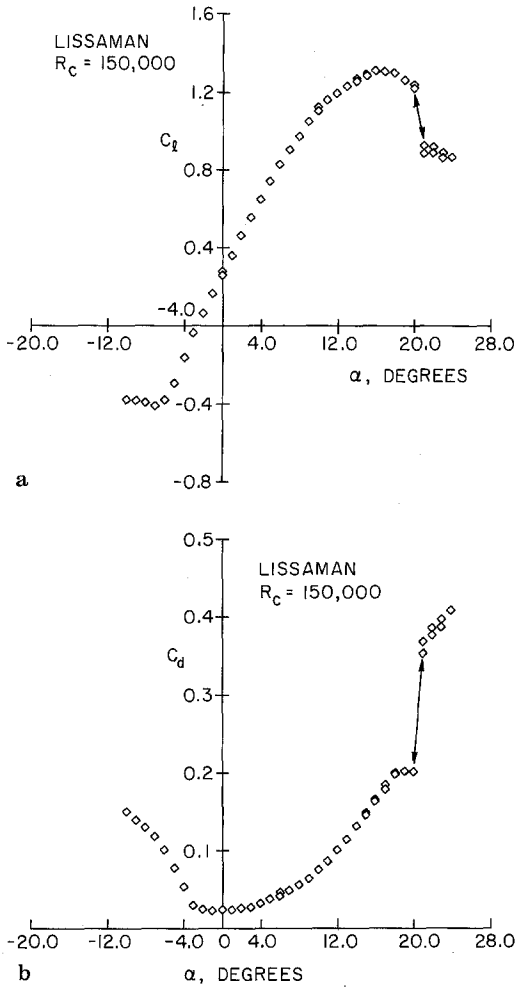

Fig. 19a and b. Lift and drag coefficients versus angle of attack of the smooth Lissaman airfoil with one 7.09 meshes/cm screen and no flow restrictor; **a** section lift coefficient; **b** section profile drag coefficient

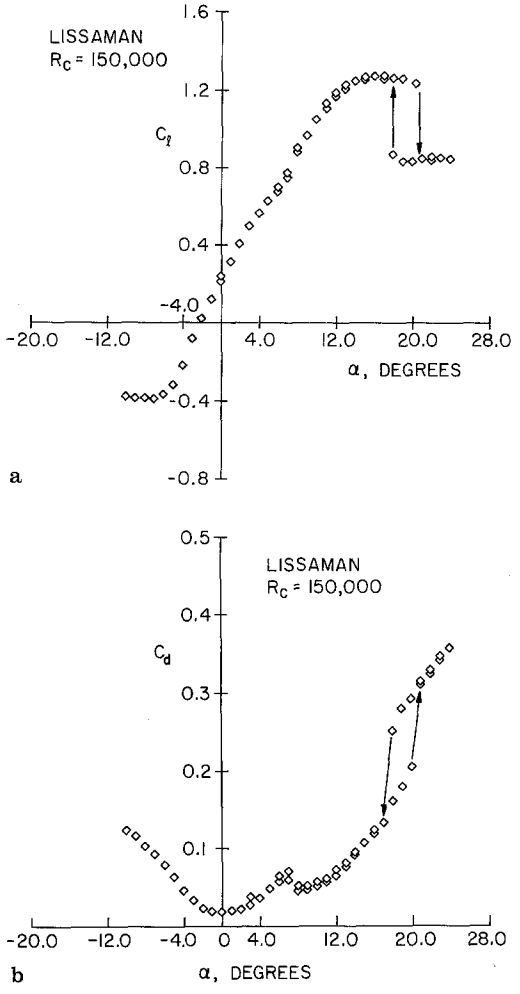

Fig. 20a and b. Lift and drag coefficients versus angle of attack of the Lissaman airfoil with tape trip at 1.1% chord and no screen or flow restrictor; **a** section lift coefficient; **b** section profile drag coefficient

Free-stream disturbances are a major source of disparity in experimental data. However, there are other sources of disparity which produce results similar to those produced by free-stream turbulence. Figures 20a and 20b show the lift and drag curves produced in the standard wind tunnel environment with a strip of tape 2.5 mm wide and 0.15 mm thick placed near the leading edge (i.e. across the span at 1.1% chord) of the airfoil. This small boundary layer trip reduced the hysteresis in a similar manner to the introduction of a flow restrictor. The tape produces similar results by tripping the boundary layer and causing early transition. A model with a small amount of surface roughness or irregularities in the surface caused by fabrication defects could produce the same results.

5 Concluding Remarks

The problems associated with obtaining accurate wind tunnel data for airfoil sections at low Reynolds numbers are compounded by the extreme sensitivity of the boundary layers to the free stream disturbance environment. The effect of free stream disturbances varies with magnitude, frequency content, and source of the disturbance. The sensitivity and accuracy of the measurement and data acquisition systems as well as the experimental procedure used can have a substantial effect on the results obtained.

Although free-stream disturbances produced the largest disparity between different tests for the Lissaman airfoil, not all of the differences can be attributed to free-stream disturbances. Model imperfections or surface roughness can produce results identical to those achieved with free stream disturbances. Reynolds number effects are critical at low speeds. An increase in Reynolds number from 150,000 to 200,000 will eliminate a major portion of the hysteresis, and the hysteresis is insignificant at 300,000. It is important that the free-stream disturbances be well documented for each test condition in order to correctly attribute differences in test results to these free stream

disturbances. A clear distinction between the effects of free-stream disturbances, model irregularities, and Reynolds number must be made before the performance of airfoils at these Reynolds numbers can be clearly understood.

This investigation indicates that it should not be surprising that different low Reynolds number results are obtained from different wind tunnel laboratories.

Acknowledgements

This research was sponsored by NASA Langley Research Center under Grant No. NSG 1419, U.S. Naval Research Laboratory under Contract No. N00014-81-K-2036 and the Department of Aerospace and Mechanical Engineering, University of Notre Dame. The authors would like to thank M. G. Kinsella and E. J. Tich for their help in obtaining the force data.

References

Bruel and Kjaer 1960: Instructions and applications manual for condenser microphones type 4133/4134. Bruel and Kjaer

Burke, J. D. 1980: The gossamer condor and albatross: a case study in aircraft design. AIAA prof. study series, Rep. no. AV-R-80/540

Conigliaro, P. E. 1983: An experimental investigation of the low Reynolds number performance of the Lissaman 7769 airfoil. AIAA Paper No. 83-0647

Jansen, B. J.; Jr. 1982: Experimental studies of the effect of the laminar separation bubble on the performance of a NACA 66_3-018 airfoil at low Reynolds numbers. M.S. Thesis, Univers. of Notre Dame

Kegelman, J. T. 1982: Experimental studies of boundary layer transition on a spinning and non-spinning axisymmetric body. Ph.D. Diss., Univ. of Notre Dame

Miley, S. J. 1972: An analysis of the design of airfoil sections for low Reynolds numbers. Ph.D. Diss. Mississippi State Univers.

Mueller, T. J.; Batill, S. M. 1982: Experimental studies of separation on a two-dimensional airfoil at low Reynolds numbers. J. AIAA 20, 457–463

Mueller, T. J.; Jansen, B. J. Jr. 1982: Aerodynamic measurements at low Reynolds numbers. AIAA paper no. 82-0598

Mueller, T. J. 1979: Smoke visualization of subsonic and supersonic flows (the legacy of F. N. M. Brown). Univ. of Notre Dame, UNDAS-TN-3412-1

Rogers, E. W. E. 1966: Blockage effects in closed or open tunnels. Agardograph 109, 279–340

Schlichting, H. 1979: Boundary layer theory. 7th ed. New York: McGraw-Hill

Received November 3, 1982